Upregulation of cytochrome c oxidase subunit 6b1 enhances mitochondrial respiration and oxidative stress response: Roles of Cox6b1 in the formation of respiratory supercomplexes and in the anti-aging effects of calorie restriction

Sang Eun Kim[1], Ryoichi Mori[1], Toshimitsu Komatsu[1], Takuya Chiba[1, 2], Hiroko Hayashi[1], Seongjoon Park[1], Michiru D. Sugawa[3,4], Norbert A. Dencher[4] and Isao Shimokawa[1]

[1]Department of Pathology, Nagasaki University School of Medicine and Graduate School of Biomedical Sciences, 1-12-4 Sakamoto, Nagasaki 852-8523, Japan

[2]Biomedical Gerontology Laboratory, Faculty of Human Sciences, and Institute of Applied Brain Sciences, Waseda University, Tokorozawa 359-1192, Japan

[3]Clinical Neurobiology, Department of Psychiatry, CBF, Charité – Universitätsmedizin Berlin, D-14050 Berlin, Germany

[4]Physical Biochemistry, Department of Chemistry, Technische Universität Darmstadt, Petersenstrasse 22, D-64287 Darmstadt, Germany

Short title: Roles of Cox6b1 in mitochondrial functions

Correspondence should be addressed to
Isao Shimokawa, M.D., PhD.
Department of Pathology
Nagasaki University School of Medicine and Graduate School of Biomedical Sciences
1-12-4 Sakamoto, Nagasaki 852-8523, Japan
Tel: +81-95-819-7051
Fax: +81-95-819-7052
E-mail: shimo@nagasaki-u.ac.jp

Abstract

Calorie restriction (CR), a non-genetic intervention that promotes longevity in animals, may exert anti-aging effects by modulating mitochondrial functions. Based on our prior mitochondrial proteome analysis, we focused on the potential roles of cytochrome c oxidase (Cox) subunit 6b1, an assembly factor for Cox. In *in vitro* experiments, Cox6b1-overexpressing NIH3T3 cells showed increased oxygen consumption rates, Cox activity, and intracellular ATP concentrations, indicating enhanced mitochondrial respiration, compared with control (Con)-3T3 cells. Despite the increased basal level of mitochondrial reactive oxygen species (ROS), cell viability after inducing oxidative stress was greater in Cox6b1-3T3 cells than in Con-3T3 cells, probably because of prompt activation of protective mechanisms, such as nuclear translocation of nuclear factor E2-related factor-2. Blue-native polyacrylamide gel electrophoresis followed by immunoblotting showed a greater abundance of Cox4 and Cox6b1 in the region of high molecular weight supercomplexes in Cox6b1-3T3 cells than in Con-3T3 cells, which suggests that Cox6b1 promotes the formation of Cox supercomplexes. In mouse liver, 30% CR upregulated the amount of Cox6b1 and increased the proportion of supercomplexes composed of Complexes I, III, and IV. The present study revealed that Cox6b1 is involved in mitochondrial functions by promoting the formation of respiratory supercomplexes and that Cox6b1 contributes to the anti-aging effects of CR.

Keywords: Calorie restriction, Cytochrome c oxidase, Cox6b1, Supercomplex

Introduction

Modest restriction of caloric intake with essential nutrients, referred to as calorie restriction (CR), increases the lifespan of a range of organisms, including the replicative lifespan of yeasts (Mair et al. 2008). The effects of CR have also been tested in non-human primates and the results to date suggest that CR extends the disease-free lifespan in monkeys, but may not increase overall survival (Colman et al. 2009; Mattison et al. 2012). This implies that we could apply the CR paradigm to prolong a healthy lifespan in humans by preventing age-related disorders. Although our knowledge of the mechanisms underlying the effects of CR is increasing, our understanding of the process remains incomplete, particularly in mammals.

Mitochondria are dynamic organelles that play critical roles in energy production, generation of reactive oxygen species (ROS), apoptosis, and intracellular signaling (Finley et al. 2012). CR may affect mitochondrial bioenergetics by modulating the composition of the mitochondrial respiratory chains. CR is thought to increase mitochondrial biogenesis in rat hepatocytes and human skeletal muscle (Lopez-Lluch et al 2006; Anthony 2007). However, Hancock et al. (2011) reported that 30% CR for 3 months did not significantly affect the protein expression of mitochondrial respiratory complexes in multiple tissues in rats. Our mitochondrial proteome analysis of the rat liver demonstrated that CR altered the expression levels of multiple subunits of respiratory chain complexes I and IV. Complex IV (cytochrome c oxidase, Cox) is thought to be a rate-limiting component of respiratory chain activity *in vivo* (Kadenbach 2003). CR decreased the expression of two subunits of Cox, namely Cox2 and Cox5a, but modestly increased the expression of one subunit, Cox6b1 (Dani et al. 2010). In the present study, we focused on Cox6b1, a non-transmembrane subunit of Cox that faces the mitochondrial intermembrane space and seems to stabilize Cox dimerization along with Cox6a (Tsukihara et al. 1996; Yoshikawa et al. 1998). In mammalian mitochondria, up to four copies of Cox are assembled into supercomplexes consisting of complexes I and III (Schägger and Pfeiffer 2000). It is thought that the formation of supercomplexes is associated with structural stabilization, increased electron transport, sequestration of reactive intermediates, and prevents excess ROS generation (Genova et al. 2014). Although an earlier study suggested that removing Cox6b1 from the purified bovine complex substantially

increased Cox activity (Weishaupt et al. 1992), a recent study showed that mutations of the Cox6b1 gene cause severe infantile encephalopathy because of inadequate Cox activity (Massa et al. 2008). Therefore, Cox6b1 may play a role in CR-specific regulation of mitochondrial bioenergetics via the assembly of respiratory supercomplexes rather than biogenesis.

In the present study, we examined whether upregulation of Cox6b1 in cells modulates mitochondrial functions and stress resistance, because stress resistance is an important feature of CR (Masoro 2003). Finally, we assessed the formation of mitochondrial supercomplexes in Cox6b1-overexpressing cells and CR mouse tissues.

Materials and methods

The animal care and experimental protocols of the present study were approved by the Ethics Review Committee for Animal Experimentation at Nagasaki University.

Materials

The following monoclonal or polyclonal antibodies (mAbs or pAbs) were used for immunoblotting: Total OXPHOS Rodent WB Antibody Cocktail (ab110413) containing five anti-mouse mAbs against 20kda subunit of complex I (NDUFB8), complex II-30kda subunit (SDHB), complex III- Core protein 2 (Core2), complex IV subunit 1(Cox1) and complex V alpha subunit (ATP5A), mouse anti-Cox6b1 mAb (ab110266), rabbit anti-Cox6b1 mAb (ab137089), mouse anti-Cox4 mAb (ab33985), rabbit anti-human nuclear factor E2-related factor-2 (Nrf2) mAb, mouse anti-human NAD(P)H:quinone oxidoreductase 1 (NQO1) mAb (ab28947), rabbit anti-VDAC/Porin pAb (ab34726), rabbit anti-mouse lamin B1 pAb (ab16048), rabbit anti-GAPDH conjugated with HRP pAb (ab9385) and rabbit anti-β-actin pAb (ab13822, Abcam, Cambridge, UK). Horseradish peroxidase-conjugated anti-rabbit or anti-mouse IgG mAbs (GE Healthcare Lifescience, Piscataway, NJ, USA) and donkey alkaline phosphatase-conjugated anti-mouse IgG mAb (Cell Signaling Technology, Danvers, MA, USA) were used to visualize the proteins in the immunoblots. G418 antibiotics were purchased from Calbiochem (Merck, Darmstadt, Germany).

Plasmid construction

The sequences encoding Cox6b1 were amplified from mouse cDNA libraries generated from mouse skin samples. The forward and reverse primers for Cox6b1 were 5'-ACCATGGCTGAAGACATCAAGACT-3' and 5'-TCAGATCTTCCCAGGAAATG-3', respectively. Amplification was performed for 30 cycles with annealing at 55°C for 30 s, extension at 68°C for 1 min, and a final extension for 5 min at 68°C. The PCR products were separated by electrophoresis on a 1% agarose gel, and were stained with SYBR Gold nucleic acid gel stain (Life Technologies, Carlsbad, CA, USA) to determine the Cox6b1 PCR product size (264 bp). The cDNA fragment of Cox6b1 was cloned into a pcDNA3.3-TOPO vector (Life Technologies). The plasmid sequences were verified by automated sequencing.

Establishment of stable NIH-3T3 cells overexpressing murine Cox6b1

NIH 3T3 cells (1.5×10^5 cells/cm^2) were cultured in Dulbecco's modified Eagle's medium (Life Technologies) containing 10% fetal bovine serum, 100 U/ml penicillin, and 100 μg/ml streptomycin, overnight at 37°C under 5% CO_2. The seeded cells were counted using the Trypan blue exclusion method on a Countess Automated Cell Counter (Life Technologies). The cells were then transfected with the pcDNA3.3-Cox6b1 plasmid using Lipofectamine 2000 (Life Technologies) according to the manufacturer's instructions. After 24 h, and every 48 h thereafter for 2 weeks, the culture medium was replaced with fresh medium containing 400 μg/ml of G418 (Wako, Tokyo, Japan). Between passages 3 and 20, four pools of clones that were stably transfected with the pcDNA3.3-Cox6b1 expression vector or a control vector (pcDNA3.3-TOPO) were collected for further studies. The intensity of transfection was confirmed by quantitative real-time PCR and immunoblotting.

Quantitative real-time RT-PCR analysis

Total RNA was extracted from murine tissues (40 mg) and cultured cells using Qiazol (Qiagen, Leusden, Netherlands). Any genomic DNA contaminating the sample was digested with DNase I (Qiagen). Further purification was performed using the RNeasy Cleanup Kit

(Qiagen). One microgram of total RNA was reverse-transcribed using the High Capacity RNA-to-cDNA Kit for RT-PCR (Applied Biosystems, Foster City, CA, USA). Quantitative PCR was performed using Thunderbird SYBR qPCR Mix (Toyobo, Osaka, Japan). Gene-specific primer sets were obtained from SYBR green gene expression assays for Cox6b1 (MA035402), Cox5a (MA025060), Cox7c (MA135797) (Takara Bio, Tokyo, Japan), Cox2 (forward: AAC CGA GTC GTT CTG AT; reverse: CTA GGG AGG GGA CTG CTC AT), and Cox5b (forward: GAT GAG GAG CAG GCT ACT GG; reverse: CAG CCA AAC CAG ATG ATA). Each sample was analyzed in duplicate. Amplification and real-time detection were performed using an ABI PRISM 7900HT (Applied Biosystems). Each sample was analyzed in duplicate. The expression levels of the target genes were normalized to those of mouse GAPDH or ACTB (β-actin) as an endogenous control (Takara Bio).

Confocal microscopy

For confocal microscopy, Cox6b1-transfected NIH3T3 cells were stained with 100 nM of Mitotracker Red (Life Technologies) for 15 min, and were fixed in 4% paraformaldehyde at room temperature for 15 min. For immunostaining, the cells were blocked with Protein block serum-free reagent (Dako, Tokyo, Japan) for 1 h. The cells were immunostained with mouse Cox6b1 mAb at room temperature for 1 h. After three washes in PBS, the cells were stained with goat anti-mouse Alexa-Fluor 488-labeled secondary IgG Ab (Life Technologies) at room temperature for 1 h. The nuclei were stained with TO-PRO-3 (Life Technologies). Immunofluorescence images were obtained using a confocal laser-scanning microscope (LSM 510 META; Carl Zeiss, Jena, Germany) and the images were processed with Zen software (Carl Zeiss).

Extracellular flux assays

Oxygen consumption rates (OCR) were measured using the XFe96 Extracellular Flux Analyzer (Seahorse Bioscience. North Billerica, MA). Cells (3.0×10^5 cells/well) were incubated overnight in growth medium. At least 1 h before measurement, the cells were incubated with XF medium (non-buffered RPMI 1460 containing 25mM glucose, 2mM L-glutamine, and 1mM Sodium Pyruvate) at 37°C in a CO_2-free incubator. The OCR were

detected under basal conditions and after the application of 1 μM oligomycin, 1 μM carbonyl cyanide-p-trifluoromethoxyphenylhydrazone (FCCP), and 1 μM rotenone + 1 μM antimycin A (XF Cell Mito Stress Test Kit; Seahorse Bioscience). Each sample was analyzed six times.

Measurement of Cox and citrate synthase activity

Mitochondrial fractions were prepared from cells using a mitochondrial isolation kit (Pierce Biochemicals/Thermo Fisher Scientific, Waltham, MA, USA). Mitochondrial pellets were suspended in 200 μl of buffer (10 mM HEPES pH 7.5, 250 mm sucrose, 1 mM ATP, 80 μM ADP, 5 mM sodium succinate, 2 mM potassium phosphate, and 1 mM dithiothreitol), and were stored at −70°C until use. The protein concentrations of the mitochondrial preparations were determined using a bicinchoninic acid (BCA) protein assay kit (Pierce Biochemical/Thermo Fisher Scientific). Cox activity in mitochondrial preparations was determined using a Complex IV assay kit (CYTOCOX1; Sigma-Aldrich, St. Louis, MO, USA). The Complex IV assay is a colorimetric assay that measures the decrease in absorbance at 550 nm corresponding to the oxidation of ferrocytochrome c to ferricytochrome c by cytochrome c oxidase. The reaction rate was measured for the first 45 s of the reaction. Cox activity was normalized for citrate synthase activity, which was measured in mitochondrial preparations using a citrate synthase activity assay kit (CS0720; Sigma-Aldrich) in accordance with the manufacturer's instructions.

Measurement of intracellular ATP concentrations

The intracellular ATP concentrations were measured using an ATP Assay Kit (A22066; Invitrogen/Life Technologies). Cells were grown in a 60 mm dish to about 80% confluence, and were then harvested. The background luminescence of 100 μl of the standard reaction solution was measured using a luminometer (FLUOstar Optima; BMG Labtech GmbH, Ortenberg, Germany) and a standard curve was generated. The standard ATP concentrations were freshly prepared to measure the ATP concentration in each sample. The protein concentration of each extract was determined using the BCA protein assay kit (Pierce Biochemical/Thermo Fisher Scientific).

Determination of ROS production

Mitochondrial superoxide production, total cellular ROS, and highly reactive oxygen species (hROS) were measured using Mitosox Red (Life Technologies), 2',7'-dichlorodihydrofluorescein diacetate (DCFH-DA; Life Technologies) and hydroxyphenyl fluorescein (HPF; Life Technologies), respectively. Cells were incubated with or without 5 mM 3-nitroproprionic acid (3-NP) for 1 h. Then, the cells were rinsed twice with phenol red-free Hanks' balanced salt solution (HBSS; Life Technologies). Next, 5 μM DCFH-DA, 5 μM HPF, or 3 μM Mitosox were added to the cells, and they were incubated in HBSS for 20 min at 37°C. The stained cells were washed three times in HBSS, harvested by trypsinization and centrifugation, and resuspended in HBSS. Fluorescence was analyzed with a BD FACS Canto II flow cytometer (BD Biosciences, San Jose, CA, USA). Signals from 10,000 cells were recorded for each sample, and data were analyzed using BD FACS Diva software (BD Biosciences). Fluorescence values were standardized according to the fluorescence values of unstained control cells.

WST-1 cell viability assay

Cells were subcultured in 96-well plates. Confluent cells were deprived of serum for 24 h and were then treated with hydrogen peroxide (300, 500, or 700 μM) for 18 h. Viable adherent cells were stained with Proliferation Reagent WST-1 (Roche Diagnostics GmbH, Penzberg, Germany) for 1 h at 37°C under 5% CO_2. The WST-1 assay is based on the reduction of WST-1 by viable cells and is suitable for measuring cell proliferation, cell viability, and cytotoxicity. The reaction produces a soluble formazan salt. Absorbance was assayed at 570 nm using a microplate reader (Sunrise; Tecan, Männedorf, Switzerland).

Protein extraction and immunoblotting for Nrf2 and NQO1

Cells were subcultured in six-well plates and grown to confluence. To examine Nrf2 nuclear translocation, the medium was replaced with serum-free medium for 24 h. The cells were then treated with 50 μM *tert*-butylhydroquinone (tBHQ) for 0, 60, or 120 min. The nuclear fraction was obtained using NE-PER nuclear and cytoplasmic extraction reagents

(Thermo Fisher Scientific). To determine the expression of NQO1, a protein upregulated by Nrf2, the medium was replaced with serum-free medium for 24 h, and the cells were treated with 0 (dimethyl sulfoxide), 25 μM or 50 μM tBHQ for 24 h. M-PER reagent (Life Technologies), containing proteinase and dephosphorylation inhibitors (Thermo Fisher Scientific), was added to the harvested cells. Debris in the supernatant was removed by centrifugation at 12,000 × *g* for 15 min. Protein samples (5 μg) were separated on 4–12% NuPAGE Novex Bis-Tris gels (Life Technologies), transferred to a polyvinylidene difluoride membrane, and blotted using standard methods. Protein bands were visualized using 5-bromo-4-chloro-3-indolyl phosphate/4-nitroblue tetrazolium (Wako) or an enhanced chemiluminescence system (Thermo Fisher Scientific). Data were analyzed using Multi gauge software (Fujifilm, Tokyo, Japan).

Mouse tissues

Liver tissues were obtained from 6-month-old male C57BL/6J mice fed *ad libitum* (AL) throughout the experiments or 30% CR diets from 12 weeks of age, and were stored at −80°C until use. The tissues were used to determine the mitochondrial protein expression, mRNA expression levels *in vivo*. The mitochondrial fractions of fresh liver tissues were used in Blue Native polyacrylamide gel electrophoresis (BN-PAGE) and two-dimensional sodium-dodecyl polyacrylamide gel electrophoresis (2D-SDS-PAGE). Animal care and the 30% CR feeding regimen are described in our previous report (Yamaza et al. 2010).

BN-PAGE

BN-PAGE analysis was performed using a NativePAGE™ Novex® Bis-Tris Gel System (Life Technologies) according to the manufacturer's instructions. Mitochondrial fractions were solubilized in 1–2% digitonin and were prepared with a NativePAGE Sample Prep Kit (BN2008; Life Technologies) and separated on 3–12% NativePAGE Novex Bis-Tris Gels (BN1001BOX; Life Technologies). Bovine Heart Mitochondria WB Control (458322; Life Technologies) and NativeMark Unstained Protein Standard (LC0725; Life Technologies) were loaded as molecular mass standards. After electrophoresis, one-dimensional (1D) gels were stained with colloidal Coomassie brilliant blue G250 and SilverQuest silver staining kit

(LC6070; Life Technologies) or were transferred to polyvinylidene difluoride (PVDF) membranes for immunoblotting. For low molecular weight native proteins, proteins were transferred to the gel for 8 min using an iBlot Dry-blotting System (Life Technologies). A wet transfer system (Trans-Blot Protein Transfer System; Bio-Rad) was used to transfer high molecular weight proteins and protein complexes to the PVDF membrane at 60 V for 4 h, in accordance with the manufacturer's instructions. After protein transfer, the membranes were soaked in 8% acetic acid for 5 min and washed with distilled water for 5 min. The membranes were washed in methanol for 5 min to de-stain G-250. The membranes were then immunoblotted with antibodies.

To detect the supercomplexes using the Cox6b1 antibody, the bands thought to correspond to supercomplexes were excised with razor, chopped, and destained with 50% methanol and 5% acetic acid in deionized water at 4°C for overnight. The protein was extracted from the gel using NuPAGE® LDS Sample Buffer (NP0008; Life Technologies) containing NuPAGE® Sample Reducing Agent (NP0009; Life Technologies) at 4°C for 1 hour. The proteins were separated by SDS-PAGE and transferred to a PVDF membrane as described above. To separate proteins in the two dimensions (2D), the lane cut from BN-PAGE gel was equilibrated in NuPAGE® LDS Sample Buffer (Life Technologies) according to the manufacturer's instructions. The equilibrated gel strip was then applied to Novex® 4–12% Bis-Tris ZOOM® Protein Gels (NP0330BOX; Life Technologies) and separated by SDS-PAGE using the transfer and immunoblotting procedures described above

Data analysis

Unpaired Student's *t* test was used to determine the significance of differences between the treatment groups. Statistical significance was accepted at values of $P<0.05$.

Results

Establishment of Cox6b1-overexpressing cells

To identify a role of Cox6b1 protein, we established stable Cox6b1-overexpressing cells. Of the clones of NIH-3T3 cells showing elevated Cox6b1 protein expression, we selected one clone in which the Cox6b1 mRNA expression level was modestly (1.8 times; Cox6b1-3T3 cells) greater than that in control cells (Con-3T3) transfected with the control vector (pcDNA3.3-TOPO) (Fig. 1a). Cox6b1 overexpression did not significantly affect the expression of the other Cox subunit genes selected in the present study (Fig. 1a). Likewise, siRNA knockdown of Cox6b1 did not affect the expression levels of individual subunits (supplemental Fig. S1). Cox6b1 protein was mostly localized in mitochondria (Fig. 1b). The protein expression of Cox6b1 in the mitochondrial fraction was 2.6 times greater in Cox6b1-3T3 cells than in Con-3T3 cells (Fig. 1c). The total amount of Cox1 and Cox4 was not significantly different between Con-3T3 and Cox6b1-3T3 cells (Fig. 1b). Confocal microscopic images confirmed that Cox6b1 immunofluorescence mostly overlapped with that of Mitotracker Red, which specifically labels mitochondria (Fig. 1d). We also preliminarily confirmed that the overexpressed Cox6b1 labeled with green fluorescent protein was localized in the mitochondria (supplemental Fig. S2).

Overexpression of Cox6b1 induced mitochondrial respiration and stress resistance

Mitochondrial functions are tightly linked with the regulation of cellular energy metabolism, apoptosis, and ROS production. In the present study, we investigated mitochondria respiration in Cox6b1-3T3 cells, by assessing the OCR. We found that the basal OCR was slightly higher in Cox6b1-3T3 cells than in Con-3T3 cells (Fig. 2a, b). Coupled respiration—OCR linked to ATP generation—and spare respiratory capacity (SRC), which is the additional mitochondrial capacity available in response to increased workload or stress, were also increased in Cox6b1-3T3 cells compared with Con-3T3 cells. Uncoupled respiration, which indicates proton leak state of respiration, was not significantly different between Cox6b1-3T3 and Con-3T3 cells. Cox activity and cellular ATP concentrations were greater in Cox6b1-3T3 cells than in Con-3T3 cells (Fig. 2c,d). These findings indicate that oxidative phosphorylation is elevated in Cox6b1-3T3 cells. The basal level of mitochondrial superoxide was also greater in Cox6b1-3T3 cells than in Con-3T3 cells (Fig. 2e). The viability of Cox6b1-3T3 cells following the induction of oxidative stress using hydrogen peroxide was also greater than that of Con-3T3 cells (Fig. 2f). Silencing Cox6b1 expression

using siRNA decreased Cox activity and ATP levels, and attenuated the resistance of the cells to stress (supplemental Fig. S3). The reduction of Cox6b1 expression did not affect mitochondrial superoxide levels.

We also analyzed the total ROS and hROS levels in Cox6b1-3T3 and Con-3T3 cells exposed to 3-NP, an irreversible inhibitor of succinate dehydrogenase (Complex II). The basal levels of ROS and hROS were significantly greater in Cox6b1-3T3 cells than in Con-3T3 cells (Fig. 2g). Although exposure to 3-NP significantly increased the total ROS level in both cell types, the magnitude of the increase in hROS was much smaller in Cox6b1-3T3 cells than in Con-3T3 cells.

Overexpression of Cox6b1 enhanced Nrf2-mediated stress resistance in cells

Nrf2 and FoxO1 are thought to play important roles in CR-mediated stress responses *in vivo* (Pearson et al. 2008; Yamaza et al. 2010). Because the Cox6b1-3T3 cells displayed increased ROS generation but enhanced stress resistance, we evaluated the activation of Nrf2 and FoxO1 in these cells. Subcellular fractionation and immunoblot analyses revealed that Nrf2 protein expression was significantly increased in the nuclear fraction of Cox6b1-3T3 cells. This effect occurred within 60 min after induction with tBHQ, a phase II enzyme inducer (Fig. 3a). The basal nuclear Nrf2 level was similar in Con-3T3 and Cox6b1-3T3 cells. We also confirmed that the protein expression of NQO1, which is encoded by an Nrf2 target gene, was significantly increased in Cox6b1-3T3 cells compared with Con-3T3 cells (Fig. 3b). FoxO1 was not significantly activated in this experimental setting (data not shown).

Cox6b1 overexpression enhanced the recruitment of Cox into mitochondrial supercomplexes

Current studies have indicated that the formation or stabilization of mitochondrial respiratory supercomplexes modulates mitochondrial bioenergetics (Schägger 2001). A recent study also revealed that ischemic preconditioning in the heart, which minimizes the area of myocardial infarction, increased the abundance of Cox6b1 in high molecular weight supercomplexes (Wong et al. 2010). These findings may imply a role of Cox6b1 in ischemic preconditioning. Thus, we investigated the contribution of Cox6b1 overexpression to

supercomplex assembly. Using 1D BN-PAGE and subsequent immunoblotting, we found that the abundance of Cox (identified using anti-Cox4 antibodies) was increased in high molecular weight supercomplexes, indicating that Cox is integrated into the supercomplexes (Fig. 4a). Moreover, siRNA-mediated knockdown of Cox6b1 reduced the abundance of Cox in the supercomplexes (supplemental Fig. S4). Using anti-Cox6b1 antibodies, 1D-BN-PAGE and subsequent immunoblotting revealing that Cox6b1 was detected in dimeric complex IV (IV_2) and in the late-stage intermediate complex (approximately 250 kDa). The signal intensities in these regions were greater in Cox6b1-3T3 cells than in Con-3T3 cells, whereas no signals were found in the supercomplex region (Fig. 4b). We suspected that Cox6b1 was masked in the supercomplex region or its expression was very low. Therefore, we conducted SDS-PAGE and immunoblotting using samples excised from the predicted supercomplex bands on BN-PAGE gels. Although we found no increases in ATP5A or Core2 expression levels in the supercomplex region (Fig. 4c), the expression of Cox6b1 was increased in Cox6b1-3T3 cells compared with Con-3T3 cells. We also analyzed the abundance of Cox6b1 in the supercomplexes by 2D-BN/SDS-PAGE (Supplemental Fig. S5). The ratios of the putative dimeric complex IV (IV_2*), III_2/IV, and III_2/IV_2 complexes to the other complexes, which were detected by Cox 1, Cox4, and Cox6b1 antibodies, were increased in Cox6b1-3T3 cells as compared with Con-3T3 cells. Taken together, these findings suggest that Cox6b1 promotes the assembly of high molecular weight supercomplexes.

Long-term CR promoted supercomplex formation

Some controversial findings have been reported regarding the effects of CR on mitochondrial biogenesis (Lopez-Lluch et al. 2006; Anthony et al. 2007; Hancock et al. 2011). Our proteome analysis demonstrated that CR affected the expression of multiple subunits of Complexes I and IV (Dani et al. 2010). However, our study did not directly show that CR increased mitochondrial biogenesis in rat liver. In the present study, we reassessed mitochondrial respiratory complexes and subunits in fresh liver tissues obtained from 12-month old CR C57BL/6J male mice. First, we confirmed that the mRNA and protein expression levels of Cox6b1 were upregulated by CR in the mouse liver (Fig. 5a–c). Similar to Cox6b1-3T3 cells, the protein abundance of NDUFB8 in Complex I was significantly greater in CR mice than in AL mice (Fig. 5b,c). However, the protein expression levels of

ATP5A and Core2 were not significantly different between CR and AL mice.

To examine the effects of CR on supercomplex formation, we performed 1D BN-PAGE and subsequent immunoblotting using the mitochondrial fraction of liver tissues. The silver-stained BN-PAGE gel showed that the abundances of the supercomplex and individual complexes (i.e., V, III, IV and II) were similar between AL and CR mice (Fig. 6a, left panel). However, immunoblotting for Cox6b1 showed an increased abundance of Cox6b1 in the supercomplex region, and in complexes III_2IV_n, IV_2, and IV in CR mice (Fig. 6a, right panel). The 2D BN-PAGE and immunoblotting studies revealed that the proportion of $I/III_2/IV_n$ supercomplexes, detected using the Core2, Cox1, and Cox6b1 antibodies, was much greater in the CR liver compared with AL liver, although the dimeric form of Complex V (V_2), detected using the ATP5A antibody, was decreased by CR (Fig. 6b). These findings indicate that CR promotes the assembly of supercomplexes comprised of Complexes I, III, and IV.

Discussion

In the first part of the present study, we tested whether upregulation of Cox6b1, a subunit of Cox, affects mitochondrial respiration and then investigated its potential contribution to the anti-aging effects of CR. Upregulation of Cox6b1 increased mitochondrial respiration and ATP production, but also increased mitochondrial ROS levels. However, despite the increase in ROS levels, Cox6b1 overexpression actually enhanced cell viability under oxidative stress conditions. Regarding the mechanism involved in these protective effects against oxidative stress, we found that Nrf2 expression was enhanced in Cox6b1 cells. It was reported that Nrf2 mediates the oxidative stress response and the anti-neoplastic effects of CR (Pearson et al. 2008). Intriguingly, mitochondrial hROS levels were not significantly increased in response to 3-NP in Cox6b1-3T3 cells, although the baseline level was somewhat greater in Cox6b1-3T3 cells compared with Con-3T3 cells. These findings are consistent with the hypothesis of mitochondrial hormesis as a mechanism for CR (Ristow et al. 2010). CR was originally thought to slow aging by reducing mitochondrial ROS generation. However, recent studies have revealed that mitochondrial respiration and ROS are not necessarily decreased, but are actually increased by CR (Ristow et al. 2010). In *Caenorhabditis elegans*, pretreatment with a ROS scavenger abolished the stress-resisting

and life-extending effects of glucose restriction (Schultz et al. 2007), supporting the mitohormesis hypothesis of CR. In our previous study, hepatic mitochondrial ROS generation fluctuated during the fed–fasted cycle of the CR regimen (Hayashida et al., 2011). The ROS level decreased in the fed phase in CR rats, but increased in the fasted phase to a level similar to that in AL rats. Thus, CR does not always decrease ROS generation in rodents. Although we used an *in vitro* cellular model in the present study, the ROS level was constantly elevated, and intermittent increases in mitochondrial ROS during the feeding cycle *in vivo* may induce a hormetic response. In fact, the mitochondrial glutathione and oxidized glutathione levels were increased in the fasted phase relative to the fed phase of the CR regimen (Hayashida et al., 2011).

In ischemic preconditioned heart models, ROS are required for the cardioprotective signal (Chen et al. 1995; Baines et al. 1997). In the preconditioned heart, the amount of Cox6b1 is increased in mitochondrial supercomplexes comprising Complexes I, III, and IV (Wong et al. 2010). In the present study, we also showed that upregulation of Cox6b1 promotes the assembly of Cox (Complex IV) with Cox6b1 into respiratory supercomplexes. Therefore, the present *in vitro* experiments suggest that Cox6b1 regulates mitochondrial respiration and stress resistance by promoting the assembly of mitochondrial respiratory supercomplexes and contributes to the anti-aging effects of CR.

In the second part of the present study, we examined whether CR promotes respiratory supercomplex assembly *in vivo*. BN-PAGE and immunoblotting confirmed that the proportion of supercomplexes comprising Complexes I, III, and IV in the mitochondrial protein fraction was increased in CR mouse liver compared with control AL liver. However, the expression of NDUFB8 of Complex I, not just Cox6b1, was increased in the CR liver. *In vivo*, two studies have shown that CR upregulates mitochondrial biogenesis (Lopez-Lluch et al. 2006; Civitarese et al. 2007). Therefore, the effects of CR are not limited to Cox6b1. In fact, CR seems to influence the expression of several respiratory complexes or subunits, which promote the formation of functional supercomplexes.

The phosphorylation and dephosphorylation of specific subunits represent another mechanism capable of regulating Cox activity independently of the relative abundance of these subunits. A recent report suggested that GSK-3β phosphorylates Cox6b1 by physically interacting with Cox6b1 in the mitochondrial intermembrane space (Byun et al. 2012). Inhibition of GSK-3β by transforming growth factor-β1 resulted in the dephosphorylation of

Cox6b1 through the dissociation of GSK-3β from Cox6b1, resulting in respiratory defects, augmented ROS generation, and cellular senescence (Byun et al. 2012). In that study, the protein abundance of Cox6b1 remained constant. Our preliminary study did not reveal an interaction between Cox6b1 and GSK-3β or of Cox6b1 phosphorylation

In summary, the present study provides evidence that mitochondrial supercomplex assembly rather than mitochondrial biogenesis may explain at least some of the anti-aging effects of CR.

Figure and Legends

Fig. 1 Establishment of Cox6b1-3T3 cells. **a** Quantitative PCR analysis of the mRNA expression levels of Cox subunits, normalized for β-actin mRNA, in control NIH-3T3 cells (Con-3T3) and Cox6b1-overexpressing NIH-3T3 cells (Cox6b1-3T3). The results are presented as means ± SEM (n=6, *P<0.05). **b** Immunoblotting for Cox1, Cox4, and Cox6b1 in the cytosolic and mitochondrial fractions of Con-3T3 and Cox6b1-3T3 cells. β-actin and GAPDH were used as cytosolic markers and VDAC/Porin was used as a mitochondrial marker. **c** Relative expression of Cox6b1 as determined by densitometry of the immunoblots. Results are presented as means ± SEM (n=4, ***P<0.001). The values were normalized for those of VDAC/Porin. **d** Localization of Cox6b1 and MitoTracker Red signals in Cox6b1-3T3 cells. Confocal microscopic images of Cox6b1-3T3 cells stained with MitoTracker Red (mitochondria) and TO-PRO-3 (nuclei). Microscopic images of MitoTracker Red signals, Cox6b1 cells, and the merged signals (TO-PRO-3 and MitoTracker Red) are shown in the left, middle, and right panels, respectively

Fig. 2 Oxygen consumption rate (OCR), cytochrome c oxidase activity, ATP production, cell survival assay, and ROS production in Con-3T3 and Cox6b1-3T3 cells. **a** OCR was measured under basal conditions and after exposure to the indicated compounds using a XFe96 Extracellular Flux Analyzer, as described in the Material and Methods. **b** Basal respiration, coupled respiration, spare respiration capacity (SCR), and uncoupled respiration were calculated from the original XFe96 Extracellular Flux Analyzer data. The results are presented as means ± SEM (n=5; *P<0.05, **P<0.01, ***P<0.001 vs. Con-3T3). **c** Cytochrome c oxidase activity in isolated mitochondria from Con-3T3 and Cox6b1-3T3 cells. The results are presented as means ± SEM (n=6; **P<0.01). Citrate synthase activity was used as an internal control. **d** Relative ATP concentrations were measured using a luminescence assay and were normalized for the protein concentration in each sample. Results are presented as means ± SEM (n=6; **P<0.01). **f** Relative cellular viability following exposure to hydrogen peroxide (H_2O_2). Cell viability was measured using a WST-1 assay. Cells were exposed to 500 or 700 μM H_2O_2 for 24 h. The results are presented as means ± SEM (n=12; ***P<0.001 vs. initial fluorescence). **g** Con-3T3 and Cox6b1-3T3 cells

were exposed to DCFH-DA (left panel) or HPF (right panel) after being exposed to 1 μM 3-nitropropionic acid for 1 h. The fluorescence intensity of 10,000 cells per sample was analyzed using a FACS Canto II. The results are presented as the fold-change relative to the baseline level in Con-3T3 cells (*P<0.05, **P<0.01, ns, not significant)

Fig. 3 Cox6b1 overexpression induced Nrf2 nuclear translocation and upregulated NQO1 expression. **a** Nuclear levels of Nrf2 in Con-3T3 and Cox6b1-3T3 cells. Cells were exposed to tBHQ for 60 or 120 min, and nuclear extracts were used for immunoblotting analysis. Lamin B1 and β-actin were used as internal controls for nuclear and cytosolic proteins, respectively. **b** Nrf2-dependent antioxidant enzyme expression is increased in Cox6b1-3T3 cells. Con-3T3 and Cox6b1-3T3 were incubated with 25 or 50 μM tBHQ for 12 h, and the total cell lysates were subjected to immunoblotting for NQO1

Fig. 4 Effects of Cox6b1 overexpression on the recruitment of Cox and Cox6b1 to mitochondrial supercomplexes. BN-PAGE and immunoblotting of mitochondrial fractions from Con-3T3 and Cox6b1-3T3 cells. **a** 1D gels were stained with Coomassie R-250 (left panel) or immunoblotted with anti-Cox4 antibodies. Gels were transferred using a dry transfer system for low molecular weight native proteins (middle panel) (C, Con-3T3 cells; 6b1, Cox6b1-3T3 cells) or a wet transfer system for the high molecular weight supercomplex (right panel). **b** 1D gels were stained with Coomassie R-250 (left panel) or transferred for immunoblotting with the anti-Cox6b1 antibody (right panel). **c** Immunoblotting of ATP5A, Core2, and Cox6b1. The predicted bands for supercomplexes were excised from the BN-PAGE gels, as described in the Material and Methods. The positions corresponding to the mitochondrial supercomplexes containing high molecular weight supercomplexes, including $I/III_2/IV_n$, n=1, 2, 3, or 4 (SC); Complex V monomers (CV); Complex III dimers + Complex IV monomers or dimers (III_2IV_n, n=1 or 2); Complex IV dimers (IV_2); late-stage complex intermediate (LSIC); Complex IV monomers (CIV); incomplete Complex IV (CIV*); and Complex II monomers (CII) are shown

Fig. 5 Effect of CR on the expression of mitochondrial proteins. **a** Cox6b1 mRNA expression in the liver of mice fed AL or 30% CR for 6 months was determined by qPCR. The mRNA expression of β-actin was used as an internal control. The results are presented as means ±

SEM (n=6, *P<0.05). **b** Immunoblotting analysis of mitochondrial subunits using the indicated antibodies. **c** Densitometry of the immunoblots. The complex II subunit (30kda), SDHB was immunodetected as a loading control. The results are presented as means ± SEM (n=3, *P<0.05)

Fig. 6 CR promotes the assembly of mitochondrial supercomplexes. **a** BN-PAGE of liver tissue samples from mice fed AL or 30% CR for 6 months. Left panel, silver staining or immunoblotting with anti-Cox6b1 antibodies. Middle and right panels, The membrane was exposed for a short (middle panel) or long time (right panel). **b** 2D BN/SDS-PAGE of AL and CR liver samples. Western blotting was performed using anti-ATP5A antibodies for complex V, anti-Core2 antibodies for Complex III, anti-SDHB antibodies for Complex II, and anti-Cox1, anti-Cox4, and anti-Cox6b1 antibodies for Complex IV. The positions corresponding to the mitochondrial supercomplexes containing $I/III_2/IV_n$(a), I/III_2 (b), Complex V dimers (c) (SC); complex V monomers (CV); Complex III dimers (CIII or III_2); Complex III dimers + Complex IV monomers or dimers (III_2IV_n, n=1 or 2); Complex IV dimers (IV_2); Complex IV monomers (CIV); and Complex II monomers (CII) are shown. The values represent the signal intensities for each supercomplex relative to the total amount of all supercomplexes

References

Baines CP, Goto M, Downey JM (1997) Oxygen radicals released during ischemic preconditioning contribute to cardioprotection in the rabbit myocardium Journal of molecular and cellular cardiology 29:207-216.

Byun HO, Jung HJ, Seo YH, Lee YK, Hwang SC, Hwang ES, Yoon G (2012) GSK3 inactivation is involved in mitochondrial complex IV defect in transforming growth factor (TGF) beta1-induced senescence Exp Cell Res 318:1808-1819.

Chen W, Gabel S, Steenbergen C, Murphy E (1995) A redox-based mechanism for cardioprotection induced by ischemic preconditioning in perfused rat heart Circ Res 77:424-429.

Civitarese AE et al. (2007) Calorie restriction increases muscle mitochondrial biogenesis in healthy humans PLoS medicine 4:e76.

Colman RJ, Anderson RM, Johnson SC, Kastman EK, Kosmatka KJ, et al. (2009) Caloric restriction delays disease onset and mortality in rhesus monkeys. Science 325: 201-204.

Dani D, Shimokawa I, Komatsu T, Higami Y, Warnken U, et al. (2010) Modulation of oxidative phosphorylation machinery signifies a prime mode of anti-ageing mechanism of calorie restriction in male rat liver mitochondria. Biogerontology 11: 321-334.

Finley LW, Haigis MC (2009) The coordination of nuclear and mitochondrial communication during aging and calorie restriction. Ageing Res Rev 8: 173-188.

Genova ML, Lenaz G (2014) Functional role of mitochondrial respiratory supercomplexes. Biochimica et Biophysica Acta 1837: 427–443.

Hancock CR, Han DH, Higashida K, Kim SH, Holloszy JO (2011) Does calorie restriction induce mitochondrial biogenesis? A reevaluation FASEB J 25:785-791 doi:10.1096/fj.10-170415.

Kadenbach B (2003) Intrinsic and Extrinsic Uncoupling of Oxidative Phosphorylation. Biochimica et Biophysica Acta 1604: 77–94.

Lopez-Lluch G, Hunt, N, Jones, B, Zhu, M, Jamieson, H, Hilmer, S et al. (2006) Calorie restriction induces mitochondrial biogenesis and bioenergetic efficiency Proc Natl Acad Sci U S A 103:1768-1773.

Mair W, Dillin A (2008) Aging and survival: the genetics of life span extension by dietary restriction. Annu Rev Biochem 77: 727-754.

Masoro EJ (2003) Subfield history: caloric restriction, slowing aging, and extending life. Sci Aging Knowledge Environ 2003: RE2.

Massa V et al. (2008) Severe infantile encephalomyopathy caused by a mutation in COX6B1, a nucleus-encoded subunit of cytochrome c oxidase Am J Hum Genet 82:1281-1289.

Mattison JA, Roth GS, Beasley TM, Tilmont EM, Handy AM, et al. (2012) Impact of caloric restriction on health and survival in rhesus monkeys from the NIA study. Nature 489: 318-321.

Pearson KJ, Lewis KN, Price NL, Chang JW, Perez E, Cascajo MV, Tamashiro KL, et al. (2008) Nrf2 mediates cancer protection but not prolongevity induced by caloric restriction. Proc Natl Acad Sci U S A: 105(7):2325-30.

Ristow M, Zarse K (2010) How increased oxidative stress promotes longevity and metabolic health: The concept of mitochondrial hormesis (mitohormesis). Exp Gerontol 45: 410-418.

Schagger H. (2001) Respiratory chain supercomplexes. IUBMB Life 52: 119-128.

Schagger H, Pfeiffer K. (2000) Supercomplexes in the respiratory chains of yeast and mammalian mitochondria. EMBO J 19: 1777–1783.

Schulz TJ, Zarse K, Voigt A, Urban N, Birringer M, et al. (2007) Glucose Restriction Extends Caenorhabditis Elegans Life Span by Inducing Mitochondrial Respiration and Increasing Oxidative Stress. Cell Metabolism 6: 280–293.

Tsukihara T, Aoyama H, Yamashita E, Tomizaki T, Yamaguchi H, et al. (1996) The Whole Structure of the 13-Subunit Oxidized Cytochrome C Oxidase at 2.8 a.. Science (New York, NY) 272: 1136–1144.

Weishaupt A, Kadenbach B (1992) Selective removal of subunit VIb increases the activity of cytochrome c oxidase. Biochemistry 31: 11477-11481.

Wong R, Aponte AM, Steenbergen C, Murphy E (2010) Cardioprotection leads to novel changes in the mitochondrial proteome Am J Physiol Heart Circ Physiol 298:H75-91.

Yamaza H, Komatsu T, Wakita S, Kijogi C, et al. (2010) FoxO1 is involved in the antineoplastic effect of calorie restriction. Aging Cell, 9(3): 372–382.

Yoshikawa S, Shinzawa-Itoh K, Tsukihara T (1998) Crystal structure of bovine heart cytochrome c oxidase at 2.8 A resolution. J Bioenerg Biomembr 30: 7-14.

a

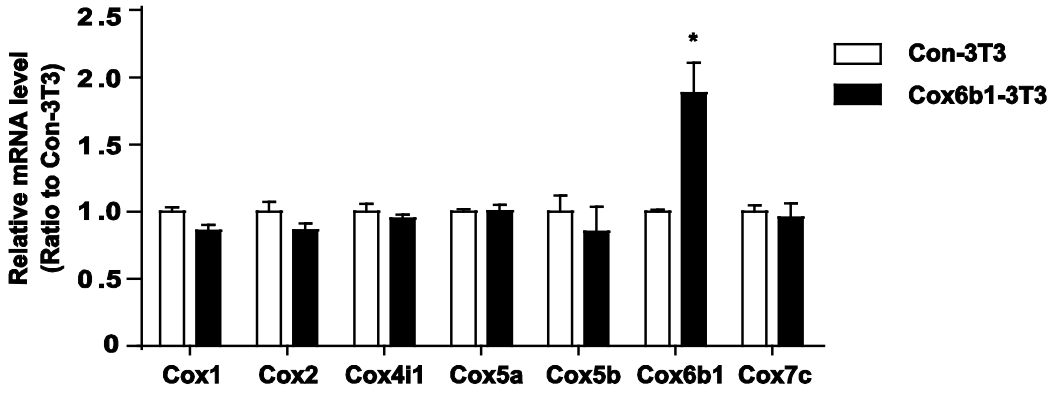
Relative mRNA level
(Ratio to Con-3T3)
2.5
2.0
1.5
1.0
0.5
0
*
Con-3T3
Cox6b1-3T3
Cox1
Cox2
Cox4i1
Cox5a
Cox5b
Cox6b1
Cox7c

b

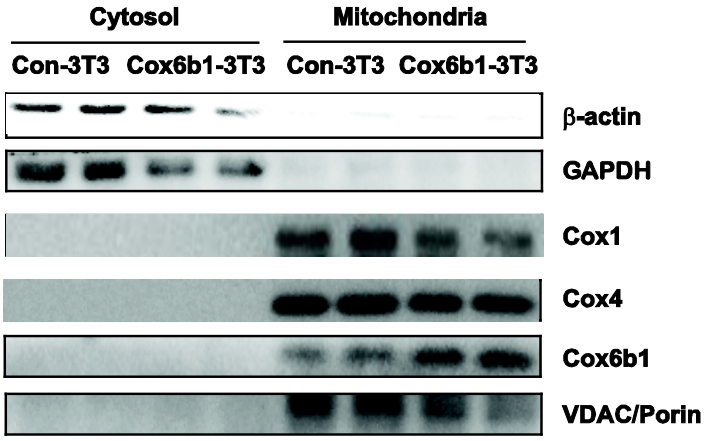
Cytosol
Mitochondria
Con-3T3
Cox6b1-3T3
Con-3T3
Cox6b1-3T3
β-actin
GAPDH
Cox1
Cox4
Cox6b1
VDAC/Porin

c

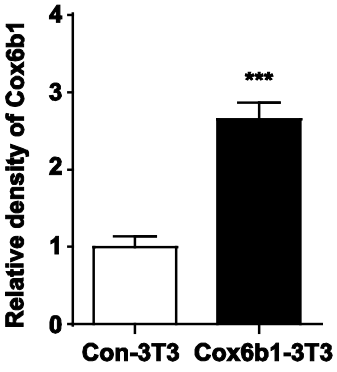
Relative density of Cox6b1
4
3
2
1
0
***
Con-3T3
Cox6b1-3T3

d

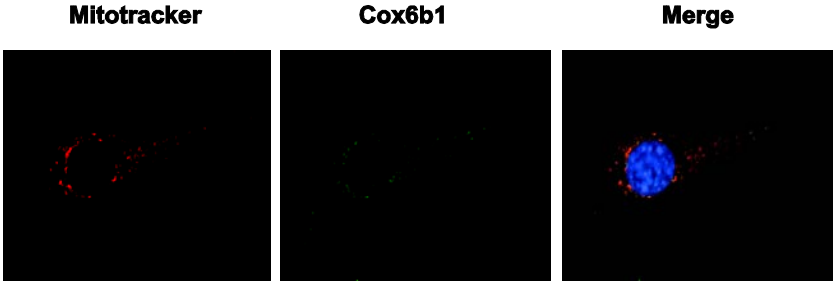
Mitotracker
Cox6b1
Merge

Fig 1

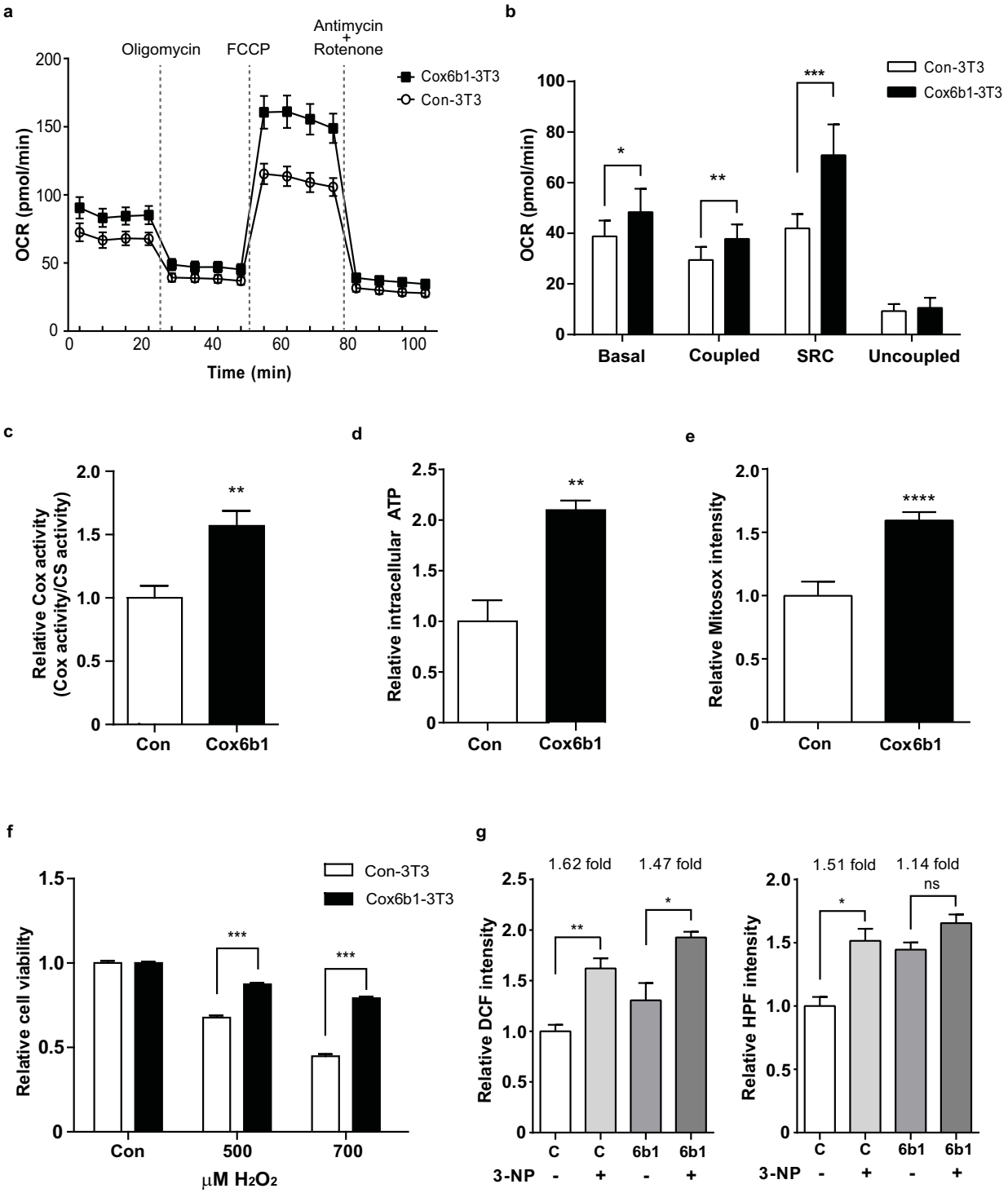
a
Oligomycin
FCCP
Antimycin + Rotenone
Cox6b1-3T3
Con-3T3
OCR (pmol/min)
Time (min)
b
Con-3T3
Cox6b1-3T3
OCR (pmol/min)
Basal
Coupled
SRC
Uncoupled
c
Relative Cox activity (Cox activity/CS activity)
Con
Cox6b1
d
Relative intracellular ATP
Con
Cox6b1
e
Relative Mitosox intensity
Con
Cox6b1
f
Con-3T3
Cox6b1-3T3
Relative cell viability
Con
500
700
μM H2O2
g
1.62 fold
1.47 fold
Relative DCF intensity
C
C
6b1
6b1
3-NP - + - +
1.51 fold
1.14 fold
ns
Relative HPF intensity
C
C
6b1
6b1
3-NP - + - +

Fig. 2

a

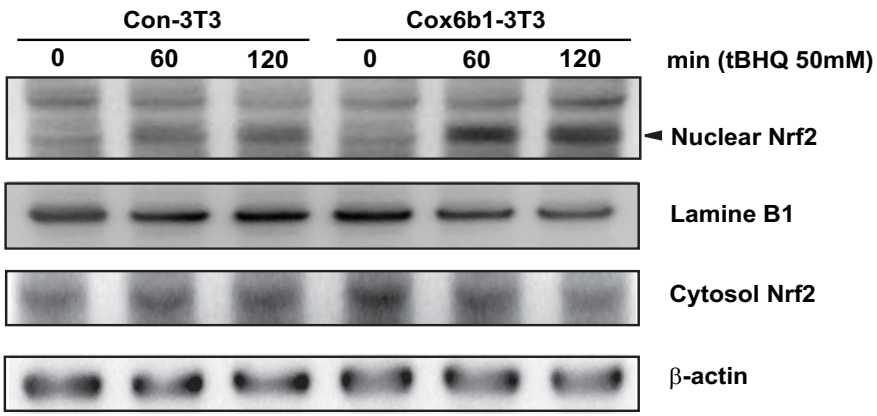
Con-3T3
Cox6b1-3T3
0
60
120
0
60
120
min (tBHQ 50mM)
Nuclear Nrf2
Lamine B1
Cytosol Nrf2
β-actin

b

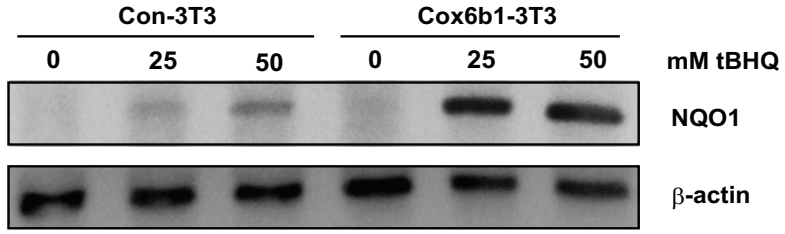
Con-3T3
Cox6b1-3T3
0
25
50
0
25
50
mM tBHQ
NQO1
β-actin

Fig 3

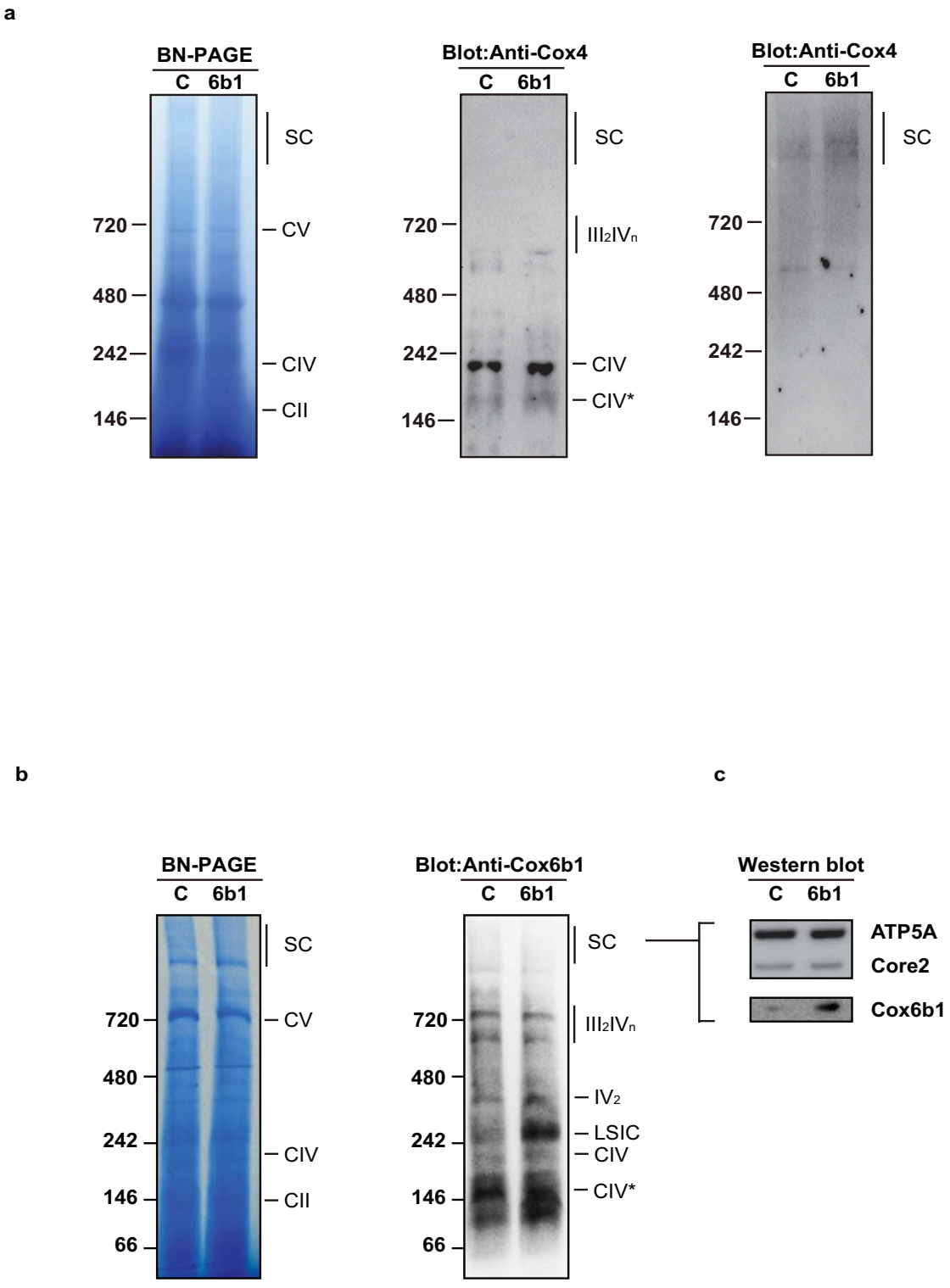
a
BN-PAGE
C 6b1
SC
720
CV
480
242
CIV
146
CII
Blot:Anti-Cox4
C 6b1
SC
720
III2IVn
480
242
CIV
CIV*
146
Blot:Anti-Cox4
C 6b1
SC
720
480
242
146
b
BN-PAGE
C 6b1
SC
720
CV
480
242
CIV
146
CII
66
Blot:Anti-Cox6b1
C 6b1
SC
720
III2IVn
480
IV2
242
LSIC
CIV
146
CIV*
66
c
Western blot
C 6b1
ATP5A
Core2
Cox6b1

Fig 4

a

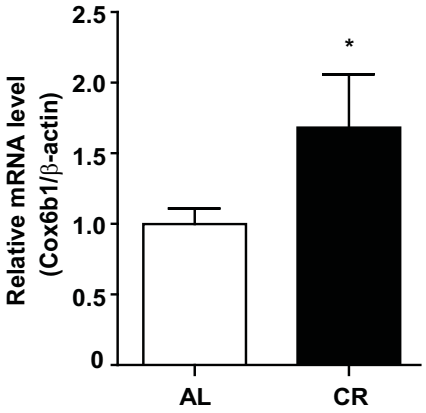
Relative mRNA level
(Cox6b1/β-actin)
2.5
2.0
1.5
1.0
0.5
0
*
AL
CR

b

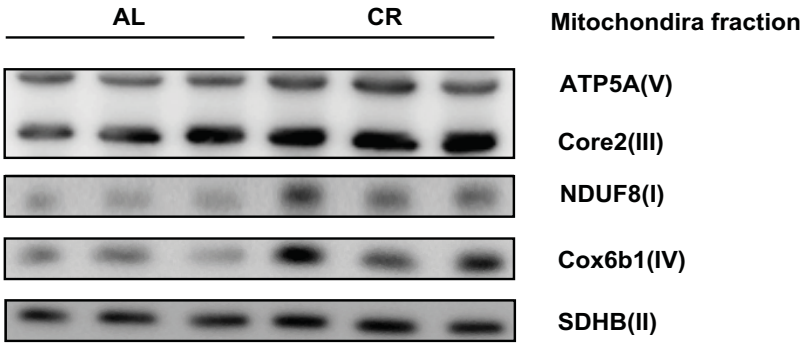
AL
CR
Mitochondira fraction
ATP5A(V)
Core2(III)
NDUF8(I)
Cox6b1(IV)
SDHB(II)

c

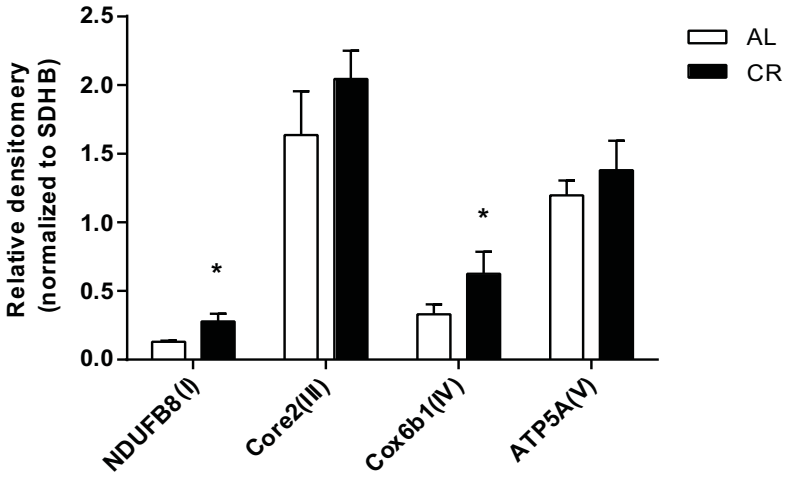
Relative densitomery
(normalized to SDHB)
2.5
2.0
1.5
1.0
0.5
0.0
*
*
AL
CR
NDUFB8(I)
Core2(III)
Cox6b1(IV)
ATP5A(V)

Fig 5

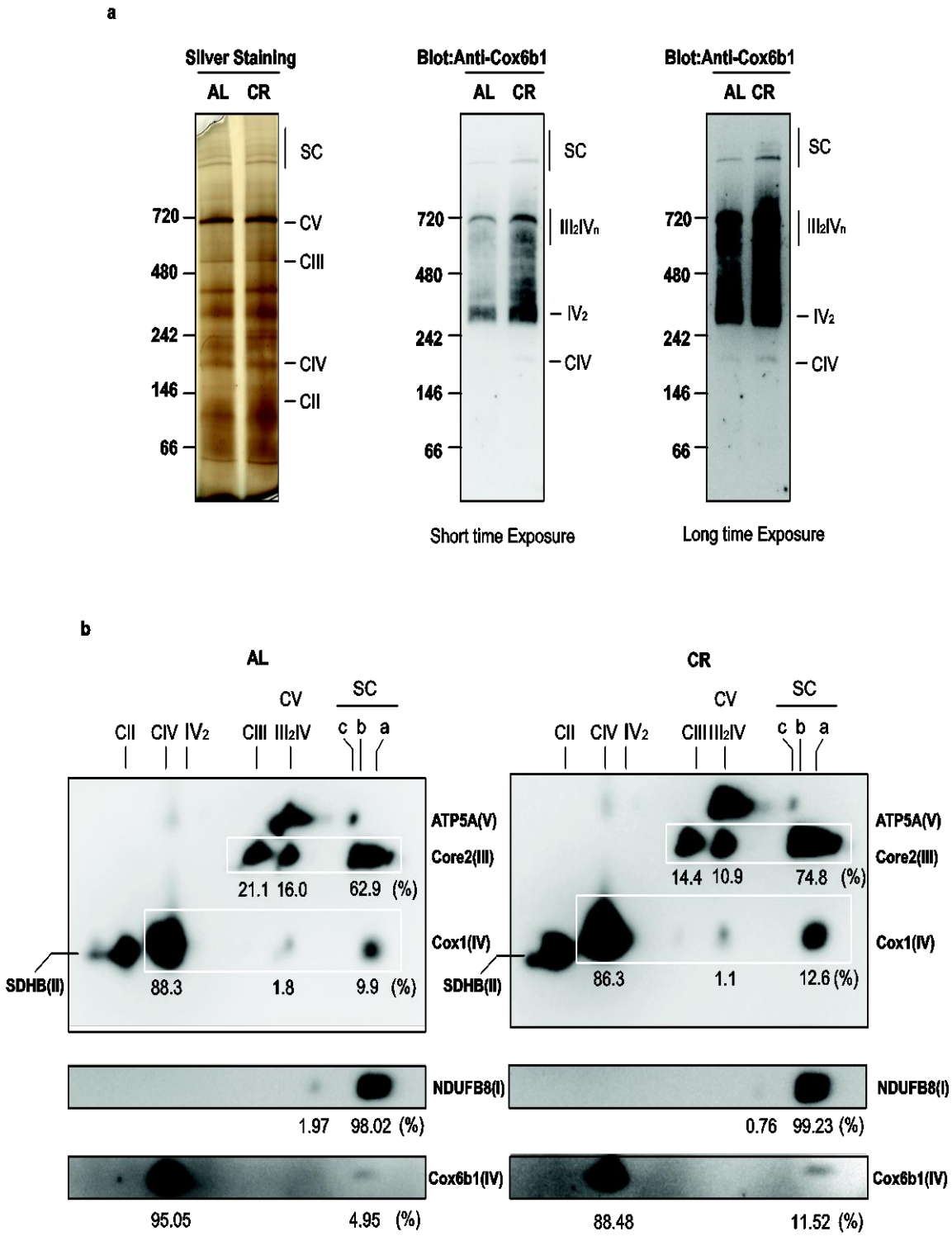
a
Silver Staining
AL CR
SC
720
480
242
146
66
CV
CIII
CIV
CII
Blot:Anti-Cox6b1
AL CR
SC
III2IVn
IV2
CIV
Short time Exposure
Blot:Anti-Cox6b1
AL CR
Long time Exposure
b
AL
CR
CII CIV IV2 CIII III2IV c b a
CV
SC
ATP5A(V)
Core2(III)
21.1 16.0 62.9 (%)
Cox1(IV)
SDHB(II)
88.3 1.8 9.9 (%)
NDUFB8(I)
1.97 98.02 (%)
Cox6b1(IV)
95.05 4.95 (%)
14.4 10.9 74.8 (%)
86.3 1.1 12.6 (%)
0.76 99.23 (%)
88.48 11.52 (%)

Fig 6